


**Direct Measurement of a Toroidally Directed Zonal Flow in a Toroidal Plasma**T. Nishizawa,<sup>1,\*</sup> A. F. Almagri,<sup>1</sup> J. K. Anderson,<sup>1</sup> W. Goodman,<sup>2</sup> M. J. Pueschel,<sup>3</sup> M. D. Nornberg,<sup>1</sup>  
S. Ohshima,<sup>4</sup> J. S. Sarff,<sup>1</sup> P. W. Terry,<sup>1</sup> and Z. R. Williams<sup>1</sup><sup>1</sup>*Department of Physics, University of Wisconsin–Madison, Madison, Wisconsin 53706, USA*<sup>2</sup>*Electrical Engineering Department, University of Wisconsin–Madison, Madison, Wisconsin 53706, USA*<sup>3</sup>*Institute for Fusion Studies, University of Texas at Austin, Austin, Texas 78712, USA*<sup>4</sup>*Institute of Advanced Energy, Kyoto University, Uji, Kyoto 611-0011, Japan* (Received 25 December 2018; revised manuscript received 16 February 2019; published 15 March 2019)

Zonal flow appears in toroidal, magnetically confined plasmas as part of the self-regulated interaction of turbulence and transport processes. For toroidal plasmas having a strong toroidal magnetic field, the zonal flow is predominately poloidally directed. This Letter reports the first observation of a zonal flow that is toroidally directed. The measurements are made just inside the last closed flux surface of reversed field pinch plasmas that have a dominant poloidal magnetic field. A limit cycle oscillation between the strength of the zonal flow and the amplitude of plasma potential fluctuations is observed, which provides evidence for the self-regulation characteristic of drift-wave-type plasma turbulence. The measurements help advance understanding and gyrokinetic modeling of toroidal plasmas in the pursuit of fusion energy.

DOI: [10.1103/PhysRevLett.122.105001](https://doi.org/10.1103/PhysRevLett.122.105001)

Achieving good confinement is necessary for fusion reactors to extract energy in a sustainable fashion. In advanced plasma confinement devices such as tokamaks and optimized stellarators, turbulent transport is typically the main contributor to the anomalously high energy and particle transport levels that have been experimentally observed [1,2]. Turbulence is a nonlinear process whose random nature is incompatible with deterministic descriptions. Even though significant progress has been made both theoretically and experimentally over the last decades toward understanding turbulent transport, further investigation is still required.

Under certain circumstances, turbulence generates zonal flows, radially localized flows with the symmetric structure in the poloidal and toroidal directions, i.e., a mode number of  $m/n = 0/0$  [3–5]. Since zonal flows are associated with localized radial electric fields, and the resulting  $E \times B$  drifts, they are poloidally directed in tokamaks and stellarators, whose magnetic field direction is mostly poloidal in the entire plasma. One example in which zonal flows may play an important role is in the initial stages of transport barrier formation. Transport barriers (TBs) locally reduce turbulent amplitudes and significantly improve the confinement [6,7]. A transition between low and high confinement ( $L$ - $H$  transition), where an edge TB appears, has been modeled by a predator-prey system in which zonal flows and equilibrium flows (predators) suppress turbulence (prey) through flow shear [7,8]. The interaction between those quantities leads to the critical energy input and bifurcation phenomena, which are the characteristics of the  $L$ - $H$  transition. However, many measurements over several devices have found that the predator-prey paradigm

is not always consistent with experimental observations, and consensus on the mechanism for the  $L$ - $H$  transition has yet to be reached [9–11]. In addition, TBs also form in the core. Zonal flows are tied to and possibly trigger this internal TB [5,12,13].

Zonal flows are a key part of self-regulated plasma turbulence. They feedback on turbulence through the sheared flow they produce and by catalyzing nonlinear energy transfer between unstable and stable modes [14]. In gyrokinetic simulations, the dominant mechanism is the zonal flow-mediated transfer of energy to stable modes, while the enhancement of turbulence decorrelation due to shearing is relatively weaker. Understanding zonal flows potentially provides a path for optimizing magnetic configurations. For instance, theoretical investigations of zonal flows in some stellarator magnetic configurations suggest zonal flows can be manipulated to control turbulence [15–17]. Moreover, a deeper understanding of the physics associated with zonal flows and their impact on transport will be helpful in the further development of other classes of fusion devices, such as tokamaks.

In this Letter, the observation of a zonal flow in the edge of a reversed field pinch (RFP) is reported for the first time. Given their importance, comprehensive understanding of zonal flows will further improve the performance of confinement devices regardless of the basic mechanisms under which they operate. To this end, it is critical to characterize zonal flows in wide parameter ranges. Measurements of zonal flows in the RFP expand the parameter range of zonal flow phenomena. In the RFP, larger magnetic shear, large magnetic fluctuation levels, and ultralow safety factor  $q$  create significant differences in zonal flow drive, sustained

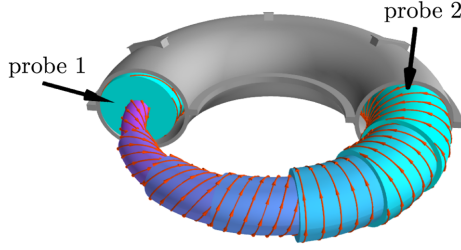


FIG. 1. Locations of the probes and magnetic configuration of a MST RFP plasma. Magnetic field lines on different flux surfaces are shown. Two black arrows indicate the locations of the probes.

zonal flow levels, and neoclassical screening, and therefore probe underlying physics. Unlike tokamaks or stellarators, the magnetic field is mostly poloidally directed in the edge, as shown in Fig. 1, and a radial electric field  $E_r$  leads to the  $E \times B$  drift in the toroidal direction. Because of the ultralow  $q$ , very high values of the Rosenbluth-Hinton (RH) zonal flow residual have been predicted in this regime [18,19]. The zonal flow residual is a measure of the ability of the plasma to maintain a zonal flow created by an impulsive perturbation. Simulations show zonal flow residuals in the RFP of  $\Phi_{\text{res}}/\Phi_0 > 0.9$ , versus values of  $\Phi_{\text{res}}/\Phi_0 < 0.2$  for tokamaks of similar aspect ratio.

The measurements are conducted on the Madison symmetric torus (MST), a RFP with major radius  $R = 1.5$  m and minor radius  $r = 0.5$  m. The last closed flux surface (LCFS) is defined by a graphite toroidal rail limiter located on the outboard midplane. In standard MST discharges, fluctuations and transport are dominated by unstable global tearing modes, a situation known to degrade zonal flow activity [20]. Tearing modes in MST can be significantly reduced by applying an inductive current profile control technique [21]. With the tearing mode amplitudes reduced, the density gradient becomes large in the edge, and density-gradient-driven trapped electron modes (TEMs) are unstable [18,22,23]. Importantly, gyrokinetic modeling indicates that electrostatic particle and electron heat transport peak at a relatively large scale for microinstabilities ( $k_y \rho_s \approx 0.2-0.4$ ) and are regulated by zonal flows [18,22]. Observations here of limit cycle behavior between the zonal flows and the turbulence provide the first experimental investigation of the regulation process in the RFP where zonal flows are also subject to degradation by magnetic fluctuations. The TEM turbulence also contributes significantly to impurity transport and probably to the bulk particle transport as well [24]. For this study, current-profile-controlled discharges with plasma current  $I_p = 200$  kA and line-averaged density  $n_e = 0.8 \times 10^{19} \text{ m}^{-3}$  are used.

The experimental setup for the zonal flow measurement and the magnetic configuration of a RFP are shown in Fig. 1. The profiles of radial electric field  $E_r$  are measured at two locations using multichannel linear capacitive probes [25], probe 1 and probe 2. Both probes are identical and have a spatial resolution of 7 mm and a

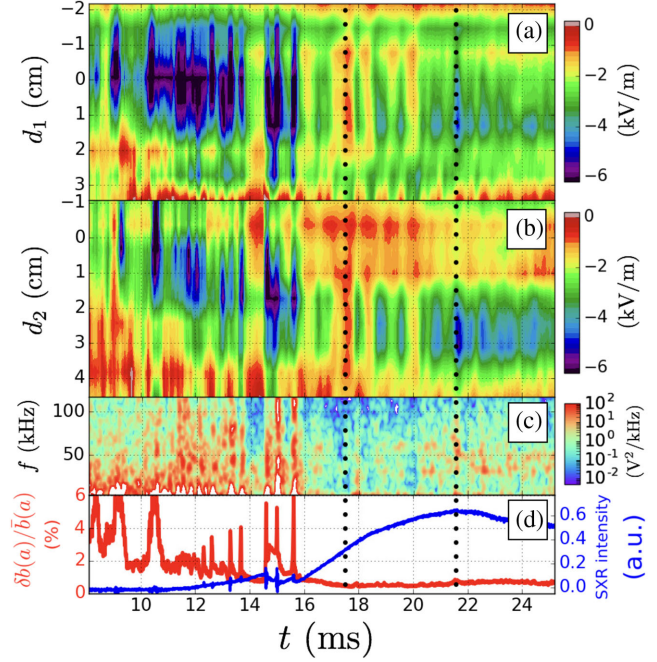


FIG. 2. (a)  $E_r$  profile measured by probe 1. (b)  $E_r$  profile measured by probe 2. (c) Spectrogram of the  $V_p$  fluctuations at  $d_1 = 1.7$  cm measured by probe 1. (d) Time evolution of the tangential magnetic fluctuations normalized by the total magnetic field at the wall and soft x-ray (SXR) emission. The time period between the black dotted lines is an example of the ranges used for the ensemble analysis.

temporal resolution of  $f_{3 \text{ dB}} = 680$  kHz. As opposed to Langmuir probes that require biased electrodes or voltage sweeping to derive the plasma potential  $V_p$ , capacitive probes are intrinsically sensitive to only  $V_p$  due to the high secondary electron generation by the boron nitride particle shield. Therefore,  $E_r$  and the associated  $E \times B$  flow can be unambiguously determined by simply evaluating the difference in the  $V_p$  measurements between adjacent electrodes. The two probes are separated by  $180^\circ$  toroidally and  $75^\circ$  poloidally.

Figures 2(a) and 2(b) show the time evolution of the  $E_r$  profiles measured by probes 1 and 2, respectively. High frequency components are removed by using a moving average filter with a width of  $200 \mu\text{s}$ . The distance measured from the LCFS is defined as  $d_1$  and  $d_2$  for probes 1 and 2, respectively, where  $d_{1,2} < 0$  cm corresponds to radial locations outside the LCFS, and  $d_1 < -1.3$  cm is inside a porthole. At 10 ms, inductive current control flattens the current gradient, and the tearing mode amplitude starts to decrease. Note that there are wells in  $E_r$  near the LCFS before 10 ms, and they move inward from 10 to 16 ms. The small inward shifts are likely due, in part, to the changing equilibrium during the inductive current profile control. Until 16 ms, the depth of the  $E_r$  well is correlated with the magnetic fluctuations. When the magnetic fluctuation amplitude spikes at a reconnection event, the  $E_r$  well becomes

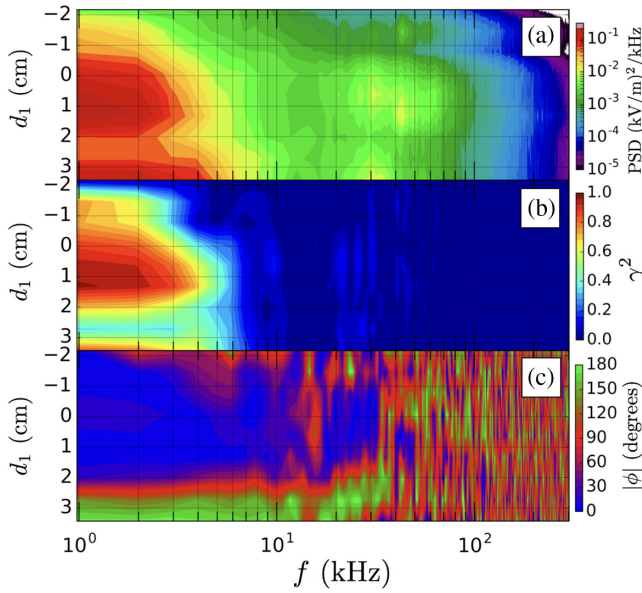


FIG. 3. (a) Profile of the power spectral density (PSD) of  $\tilde{E}_r$  in the probe 1 location. Coherence (b) and cross phase (c) between  $\tilde{E}_r$ , at the minimum of the  $E_r$  well in the probe 2 location and each  $\tilde{E}_r$  in the probe 1 location.

deeper. This relation is also observed in standard RFP plasmas without the current profile control [26]. As Fig. 2(d) shows, the tangential magnetic fluctuation amplitude stays less than 1% after 16 ms. After the suppression of magnetic fluctuations is achieved, the soft x-ray emission, which is directly related to the core electron temperature, starts to increase significantly. After 16 ms,  $V_p$  fluctuation amplitude at  $d_1 = 1.7$  cm shown in Fig. 2(c) is also reduced significantly.

In order to investigate the statistical nature of the radial electric field fluctuation  $\tilde{E}_r$ , the same time periods ( $17.5 < t < 21.6$  ms) are extracted from 19 similar discharges, and an ensemble is made. In Fig. 3(a), the power spectral density of  $\tilde{E}_r$  for the probe 1 location is shown. Near  $d_1 = 1.3$  and  $3.4$  cm, significant power is concentrated below 10 kHz with the peak near 0 Hz. The ion-ion collision frequency is estimated to be  $\sim 3$  kHz near the  $E_r$  well. Therefore, the location and width of the peak in the power spectral density are in agreement with the characteristics of a zero-mean-frequency zonal flow [27]. Figure 3(b) shows coherence  $\gamma^2$  between the minimum of the  $E_r$  well in the probe 2 location ( $d_2 = 3.1$  cm) and each  $\tilde{E}_r$  in the probe 1 location. The ensemble has 66 realizations, and the statistical significance level is  $1/66 \approx 0.015$ . The frequency components below 5 kHz are highly coherent with those of the minimum of  $E_r$  in the probe 2 location. Figure 3(c) shows the absolute values of the cross phase corresponding to Fig 3(b). The cross phase is almost zero between the minima of the  $E_r$  wells measured by probes 1 and 2 below 10 kHz. The long range correlation with the zero phase difference implies that the low frequency fluctuations ( $< 10$  kHz) have a mode

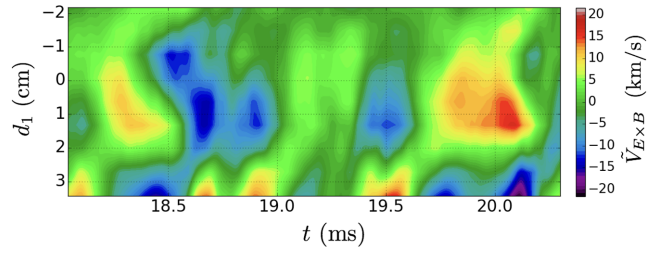


FIG. 4. The  $E \times B$  drift profile with the frequency components between 0.5 and 20 kHz. The positive velocity corresponds to the ion diamagnetic drift direction.

structure of  $m/n = 0/0$ . On the other hand, the cross phase between the  $E_r$  at  $d_1 = 3.4$  cm and the minimum of the  $E_r$  well in the probe 2 location is almost  $180^\circ$ . The ion gyroradius in the edge of these discharges is about 1.5 cm. Therefore, as one moves inward from the minimum of the  $E_r$  well by 2.5 cm, the phase of the low frequency fluctuations becomes out of phase, indicating that the radial localization of the flow at the  $E_r$  well is on the order of the ion gyroradius. Based on these observations, the  $E \times B$  flow associated with the  $E_r$  well is identified as a zero-mean-frequency zonal flow. Gyrokinetic simulations have shown that oscillatory behavior of  $V_p$  in response to a electrostatic potential perturbation, which is an indication of a geodesic acoustic mode (GAM) [28], is effectively absent for the RFP configurations [18]. Absence of a GAM in this measurement is, therefore, consistent with expectations.

The coherence  $\gamma^2$  shown in Fig. 3 starts to increase again as one passes  $d_1 = 2.7$  cm and approaches  $d_1 = 3.4$  cm in the low frequency range. The cross phase at  $d_1 = 3.4$  cm in Fig. 3(c) is near  $180^\circ$ . In addition, as can be seen Fig. 3(a), the fluctuations below 10 kHz at  $d_1 = 3.4$  cm have more power than those at the minimum of the  $E_r$  well at  $d_1 = 1.3$  cm. These observations indicate that there is another layer of a zonal flow that propagates in the opposite direction with respect to the first layer of a zonal flow near  $d_1 = 1.0$  cm. The temporal behavior of the zonal flow layers is illustrated in Fig. 4, which shows the  $E \times B$  drift velocity fluctuation  $\tilde{V}_{E \times B}$  associated with the  $E_r$  fluctuations from 0.5 to 20 kHz. Other frequency components, including equilibrium values, are filtered out. The radial structure of  $\tilde{V}_{E \times B}$  flips the sign near  $d_1 = 2.4$  cm. Since there is no external torque input, the time evolution of  $\tilde{V}_{E \times B}$  cannot be explained by a diffusive process, and there is an intrinsic torque driving the zonal flows. Radially localized  $E \times B$  flows near the LCFS are also observed in standard RFP plasmas without the current profile control. Ion orbit losses or the Reynolds stress are possible mechanisms for the edge flow formation [29,30]. However, long range correlations that indicate zonal flows are not observed in standard MST RFP discharges when the same diagnostic technique is applied [26].

The zero-mean-frequency zonal flow is observed just inside the LCFS where zonal flows undergo limit cycle

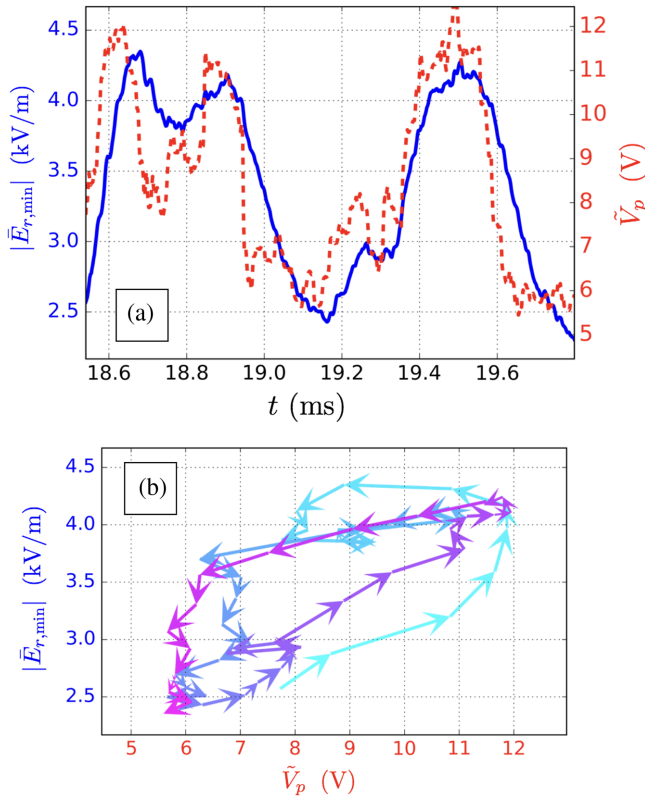


FIG. 5. (a) Time evolution of the depth of the  $E_r$  well  $|\bar{E}_{r,\min}|$  and the rms of the  $V_p$  fluctuations above 20 kHz at  $d_1 = 1.7$  cm,  $\tilde{V}_p$ . (b) The corresponding Lissajous curve. Each arrow represents a time step of 50  $\mu$ s.

oscillations prior to the  $L$ - $H$  transition of tokamaks in the predator-prey system [8]. The zonal flow in the RFP is also found to execute limit cycle oscillations. Figure 5(a) shows the time evolution of the depth of the  $E_r$  well  $|\bar{E}_{r,\min}|$  and the rms of the  $V_p$  fluctuations above 20 kHz at  $d_1 = 1.7$  cm,  $\tilde{V}_p$ . A moving average filter with a width of 100  $\mu$ s is applied to calculate  $|\bar{E}_{r,\min}|$ . The same time window is used to obtain  $\tilde{V}_p$ . Here,  $|\bar{E}_{r,\min}|$  is a measure of the zonal flow amplitude. In Fig. 5(b), the Lissajous curve corresponding to Fig. 5(a) is shown. First, the turbulence amplitude  $\tilde{V}_p$  increases, and the zonal flow amplitude  $|\bar{E}_{r,\min}|$  follows with a time lag of  $\sim 20^\circ$ . This oscillation involving zonal flows and plasma potential fluctuations is indicative of zonal flow regulation, but differs from the limit cycle oscillations of Ref. [7], where the zonal flow oscillation leads the oscillation of the turbulence signal by  $\sim 90^\circ$ . This difference suggests that the dynamics may be affected by processes not incorporated in existing models of the  $L$ - $H$  transition [8]. Such processes might include the strong RH residual associated with ultralow  $q$ , the high sensitivity of density-gradient-driven TEM to zonal flows [18], the degradation of zonal flows by the reduced but nonzero global magnetic fluctuations of current-profile-controlled RFP plasmas [18,20,22,31], and energy transfer to large-scale stable modes.

In summary, the observation of a zonal flow that is directed primarily in the toroidal direction is reported for the first time in a toroidal magnetically confined plasma. The radial electric field profiles are measured using two multichannel linear capacitive probes in the edge of a reversed field pinch plasma for which a high Rosenbluth-Hinton residual is predicted. Clear experimental evidence of a zonal flow is provided based on the long-range correlation consistent with the mode structure of  $m/n = 0/0$  and the radial localization of the  $E \times B$  flow. Gyrokinetic modeling of these discharges has shown that trapped-electron mode turbulence is present and drives zonal flows, indicating that the turbulence is regulated by the zonal flows. Limit cycle oscillations involving the zonal flow and plasma potential fluctuations are observed, providing information about the regulation process. The phase characteristics of the limit cycle differ from those observed in early stage  $L$ - $H$  transitions, suggesting that additional effects in zonal flow regulation present in the reversed field pinch affect predator-prey dynamics. Further studies are necessary to understand the precise interplay between zonal flows, turbulence, stable modes, and global magnetic fluctuations. Multiscale interactions, as they appear in MST plasmas, provide experimental impetus to go beyond plasma modeling that has typically been isolated to large- (e.g., magnetohydrodynamics) or small-scale (e.g., gyrokinetic) analysis.

Data shown in this Letter can be obtained in Supplemental Material [32].

The authors would like to thank J. Smoniewski and D. M. Kriete for valuable discussions. This work is supported by the U.S. Department of Energy, Office of Science, and Office of Fusion Energy Sciences under Awards No. DE-FG02-05ER54814 and No. DE-FG02-04ER-54742.

\*Current address: Max-Planck-Institut für Plasmaphysik, Greifswald, Germany.  
takashi.nishizawa@ipp.mpg.de

- [1] G. R. Tynan, A. Fujisawa, and G. McKee, *Plasma Phys. Controlled Fusion* **51**, 113001 (2009).
- [2] W. Horton, *Rev. Mod. Phys.* **71**, 735 (1999).
- [3] A. Fujisawa *et al.*, *Nucl. Fusion* **47**, S718 (2007).
- [4] A. Hasegawa and M. Wakatani, *Phys. Rev. Lett.* **59**, 1581 (1987).
- [5] A. Fujisawa *et al.*, *Phys. Rev. Lett.* **93**, 165002 (2004).
- [6] F. Wagner *et al.*, *Phys. Rev. Lett.* **53**, 1453 (1984).
- [7] L. Schmitz, L. Zeng, T. L. Rhodes, J. C. Hillesheim, E. J. Doyle, R. J. Groebner, W. A. Peebles, K. H. Burrell, and G. Wang, *Phys. Rev. Lett.* **108**, 155002 (2012).
- [8] E.-J. Kim and P. H. Diamond, *Phys. Rev. Lett.* **90**, 185006 (2003).
- [9] T. Kobayashi, K. Itoh, T. Ido, K. Kamiya, S.-I. Itoh, Y. Miura, Y. Nagashima, A. Fujisawa, S. Inagaki, K. Ida, and K. Hoshino, *Phys. Rev. Lett.* **111**, 035002 (2013).

- [10] S. J. Zweben, R. J. Maqueda, R. Hager, K. Hallatschek, S. M. Kaye, T. Munsat, F. M. Poli, A. L. Roquemore, Y. Sechrest, and D. P. Stotler, *Phys. Plasmas* **17**, 102502 (2010).
- [11] C. S. Chang, S. Ku, G. R. Tynan, R. Hager, R. M. Churchill, I. Cziegler, M. Greenwald, A. E. Hubbard, and J. W. Hughes, *Phys. Rev. Lett.* **118**, 175001 (2017).
- [12] R. E. Waltz, M. E. Austin, K. H. Burrell, and J. Candy, *Phys. Plasmas* **13**, 052301 (2006).
- [13] M. W. Shafer, G. R. McKee, M. E. Austin, K. H. Burrell, R. J. Fonck, and D. J. Schlossberg, *Phys. Rev. Lett.* **103**, 075004 (2009).
- [14] K. D. Makwana, P. W. Terry, M. J. Pueschel, and D. R. Hatch, *Phys. Rev. Lett.* **112**, 095002 (2014).
- [15] H. Sugama and T.-H. Watanabe, *Phys. Plasmas* **13**, 012501 (2006).
- [16] P. Xanthopoulos, A. Mischchenko, P. Helander, H. Sugama, and T.-H. Watanabe, *Phys. Rev. Lett.* **107**, 245002 (2011).
- [17] C. C. Hegna, P. W. Terry, and B. J. Faber, *Phys. Plasmas* **25**, 022511 (2018).
- [18] Z. R. Williams, M. J. Pueschel, P. W. Terry, and T. Hauff, *Phys. Plasmas* **24**, 122309 (2017).
- [19] I. Predebon and P. Xanthopoulos, *Phys. Plasmas* **22**, 052308 (2015).
- [20] P. W. Terry, M. J. Pueschel, D. Carmody, and W. M. Nevins, *Phys. Plasmas* **20**, 112502 (2013).
- [21] J. K. Anderson *et al.*, *Phys. Plasmas* **12**, 056118 (2005).
- [22] D. Carmody, M. J. Pueschel, J. K. Anderson, and P. W. Terry, *Phys. Plasmas* **22**, 012504 (2015).
- [23] J. R. Duff, Z. R. Williams, D. L. Brower, B. E. Chapman, W. X. Ding, M. J. Pueschel, J. S. Sarff, and P. W. Terry, *Phys. Plasmas* **25**, 010701 (2018).
- [24] T. Nishizawa, M. D. Nornberg, J. Boguski, D. J. Den Hartog, J. S. Sarff, Z. R. Williams, Z. A. Xing, and D. Craig, *Phys. Rev. Lett.* **121**, 165002 (2018).
- [25] T. Nishizawa, A. F. Almagri, W. Goodman, S. Ohshima, and J. S. Sarff, *Rev. Sci. Instrum.* **89**, 10J118 (2018).
- [26] T. Nishizawa, Characterizing the Role of Drift-Wave Turbulence in a Reversed Field Pinch, Ph. D. thesis, University of Wisconsin, Madison, WI, 2018.
- [27] D. K. Gupta, R. J. Fonck, G. R. McKee, D. J. Schlossberg, and M. W. Shafer, *Phys. Rev. Lett.* **97**, 125002 (2006).
- [28] K. J. Zhao, T. Lan, J. Q. Dong, L. W. Yan, W. Y. Hong, C. X. Yu, A. D. Liu, J. Qian, J. Cheng, D. L. Yu, Q. W. Yang, X. T. Ding, Y. Liu, and C. H. Pan, *Phys. Rev. Lett.* **96**, 255004 (2006).
- [29] V. Antoni, D. Desideri, E. Martines, G. Serianni, and L. Tramontin, *Phys. Rev. Lett.* **79**, 4814 (1997).
- [30] N. Vianello, E. Spada, V. Antoni, M. Spolaore, G. Serianni, G. Regnoli, R. Cavazzana, H. Bergsäter, and J. R. Drake, *Phys. Rev. Lett.* **94**, 135001 (2005).
- [31] M. J. Pueschel, P. W. Terry, F. Jenko, D. R. Hatch, W. M. Nevins, T. Görler, and D. Told, *Phys. Rev. Lett.* **110**, 155005 (2013).
- [32] See Supplemental Material at <http://link.aps.org/supplemental/10.1103/PhysRevLett.122.105001> for data shown in this Letter.